University of Cologne, Institute of Geography; China Agricultural University, Department of Plant Nutrition

VERY HIGH RESOLUTION CROP SURFACE MODELS (CSM) FROM UAV-BASED STEREO IMAGES FOR RICE GROWTH MONITORING IN NORTHEAST CHINA

Juliane Bendig, Maximilian Willkomm, Nora Tilly, Martin Leon Gnyp, Simon Bennertz, Victoria I. S. Lenz-Wiedemann, Georg Bareth, Yuxin Miao

Abstract: Unmanned Aerial Vehicles (UAV) became popular platforms for the collection of remotely sensed geodata in the last years (Hardin & Jensen 2011). Various applications in numerous fields of research like archaeology (Hendrickx et al. 2011), forestry or geomorphology evolved (Martinsanz 2012). This contribution deals with the generation of very high resolution multi-temporal Crop Surface Models (CSM) for rice growth monitoring by means of low-cost equipment. The concept of the generation of multi-temporal CSM using terrestrial Laserscanning (TLS) has already been introduced by Hoffmeister et al. (2010). For this study, data acquisition was performed with a low-cost and low-weight Mini-UAV (< 5 kg). UAV in general and especially smaller ones, like the system presented here, close a gap in small scale remote sensing (Berni et al. 2009, Watts et al. 2012). In precision agriculture frequent remote sensing on such scales during the vegetation period provides important spatial information on the crop status. Crop growth variability can be detected by comparison of the CSM in different phenological stages. In this contribution, the method, that has already been used for barley (Bendig et al. 2013), is applied to a different crop in a different environment. The study area is an experiment field for rice in Northeast China (Sanjiang Plain). Two rice cultivars were planted and treated with different amounts of N-fertilizer. In July 2012 three UAV-campaigns were carried out. Additionally, further destructive and non-destructive field data were collected. The UAV-system is an MK-Okto by Hisystems (www.mikrokopter.de) equipped with a high resolution optical consumer camera. The self-built and self-maintained system has a payload of up to 1 kg and 15 minutes mean endurance and can be operated up to a wind speed of less than 19 km/h. Stereo images were captured at a flying height of 50 m and a 44% side and 90% forward overlap. The images are processed into CSM under the use of the Structure from Motion (SfM)-based software Agisoft Photoscan 0.9.0. The resulting models have a resolution of 0.02 m. Further data processing in Esri ArcGIS allows for quantitative comparison of the plant heights. The multi-temporal datasets are analysed on a plot size basis. The results can be compared to and combined with the additional field data. Detecting plant height with non-invasive measurement techniques enables analysis of its correlation to biomass and other crop parameters (Hansen & Schjoerring 2003, Thenkabail et al. 2000) measured in the field. The method presented here can therefore be a valuable addition for the recognition of such correlations.

Keywords: Agriculture, biomass, DEM, multi-temporal data, plant height, rice, UAV

HOCHAUFLÖSENDE CROP SURFACE MODELS (CSM) AUF DER BASIS VON STEREOBILDERN AUS UAV-BEFLIEGUNGEN ZUR ÜBERWACHUNG VON REISWACHSTUM IN NORDOSTCHINA

Zusammenfassung: Unmanned Aerial Vehicles (UAV) wurden in den letzten Jahren zu beliebten Plattformen für die Sammlung von mit Fernerkundungsmethoden erhobenen Geodaten (Hardin & Jensen 2011). Verschiedene Anwendungen in vielen Forschungsbereichen wie Archäologie (Hendrickx et al. 2011), Forstwirtschaft oder Geomorphologie (Martinsanz 2012) entwickelten sich. Dieser Beitrag befasst sich mit der Erzeugung von multitemporalen Crop Surface Models (CSM) mit sehr hoher Auflösung zur Überwachung von Reiswachstum mit günstiger Ausrüstung. Das Konzept der Generierung von multitemporalen CSM mittels terrestrischem Laserscanning (TLS) wurde bereits von Hoffmeister et al. (2010) eingeführt. Für diese Studie wurde die Datenerfassung mit einem günstigen und leichten Mini-UAV (< 5 kg) durchgeführt. UAV allgemein und vor allem kleinere, wie das hier vorgestellte System, schließen eine Lücke in der Fernerkundung im Nahbereich (Berni et al. 2009, Watts et al. 2012). Im Präzisionsackerbau liefern häufige Erhebungen von Fernerkundungsdaten im Nahbereich, während der Vegetationsperiode, wichtige räumliche Informationen über den Pflanzenzustand. Variabilität im Pflanzenwachstum kann durch Vergleich der CSM in verschiedenen phänologischen Stadien erkannt werden. In diesem Beitrag wird das Verfahren, welches bereits für Gerste genutzt wurde (Bendig et al. 2013), auf eine andere Feldfrucht in einer anderen Umgebung angewendet. Das Untersuchungsgebiet ist ein Versuchsfeld für Reis in Nordost-China (Sanjiangebene).

Zwei Reissorten wurden dort gepflanzt und mit unterschiedlichen Mengen Stickstoffdünger behandelt. Im Juli 2012 wurden drei UAV-Kampagnen durchgeführt. Zusätzlich erfolgte die Erhebung weiterer destruktiver und nicht destruktiver Felddaten. Das UAV-System ist ein MK-Okto von Hisystems (www.mikrokopter.de), ausgestattet mit einer hochauflösenden optischen Digitalkamera. Das selbst gebaute und selbst gewartete System hat eine Nutzlast von bis zu 1 kg, eine Flugdauer von durchschnittlich 15 Minuten und kann bis zu einer Windgeschwindigkeit von unter 19 km/h betrieben werden. Die Erfassung der Stereobilder erfolgte bei einer Flughöhe von 50 m und einer 44 % Seit- und 90 % Vorwärtsüberlappung. Die Bilder werden in CSM mittels der Structure from Motion(SFM)-basierten Software Agisoft Photoscan 0.9.0 prozessiert. Die resultierenden Modelle verfügen über eine Auflösung von 0,02 m. Weitere Datenverarbeitung in Esri ArcGIS ermöglicht quantitative Vergleiche der Pflanzenhöhen. Die multitemporalen Datensätze werden auf Basis sogenannter „Versuchsplots" analysiert. Die Ergebnisse können mit den zusätzlichen Felddaten verglichen und kombiniert werden. Die Erfassung von Wuchshöhe mit nichtinvasiven Messverfahren ermöglicht die Analyse der Korrelation zu Biomasse und anderen Pflanzenparametern, die im Feld gemessen werden (Hansen & Schjoerring 2003, Thenkabail et al. 2000). Die hier vorgestellte Methode kann somit eine wertvolle Ergänzung für die Erkennung solcher Korrelationen liefern.

Schlüsselwörter: Landwirtschaft, Biomasse, DGM, multitemporale Daten, Pflanzenhöhe, Reis, UAV

Authors

Dipl.-Geogr. Juliane Bendig
B. Sc. Maximilian Willkomm
Dipl.-Geogr. Nora Tilly
Dipl.-Geogr. Martin Leon Gnyp
Simon Bennertz
Dr. Victoria I. S. Lenz-Wiedemann
Prof. Dr. Georg Bareth
University of Cologne
Institute of Geography
GIS & Remote Sensing Group
Albertus-Magnus-Platz
D-50923 Köln
E: {juliane.bendig, m.willkomm, nora.tilly, mgnyp1, s.bennertz, victoria.lenz, g.bareth}@uni-koeln.de

Prof. Dr. Yuxin Miao
Qiang Cao
China Agricultural University
Department of Plant Nutrition
No 2, Yuanmingyuan West Road
100193 Beijing, China
E: {qiangcao, ymiao}@cau.edu.cn

1 INTRODUCTION

Surveying crop growth during phenological stages is an important component of precision agriculture (Hansen & Schjoerring 2003, Thenkabail et al. 2000). Remote sensing has great potential of contributing data for such kind of investigations in the field of precision agriculture (Mulla 2012). In Northeast China, rice production is an important economic factor and contributes to ensuring the food supply for the local population (Miao et al. 2011, Peng et al. 2006). The use of precision agriculture to optimise rice cultivation in this region has high potential. The control of plant growth can help to improve management of the fields. In experiment fields, such as the one in this contribution, the relationship between application of different amounts of N-fertilizer and plant parameters is investigated. These plant parameters can be put in relation to the size of the plant, which is related to the yield. A way to monitor plant growth is the idea of generating multi-temporal Crop Surface Models (CSM) to allow for comparison of different phenological stages (Hoffmeister et al. 2010, Bendig et al. 2013). For each date of data acquisition a model of the crop surface is generated from highly dense point clouds. The plant growth is obtained by comparison of the surface models for each date. Data collection using a mobile, low-cost and self-maintainable device like a small UAV offers big advantages in this remote region of the world. In addition, the well-managed, small-sized experiment field provides an ideal opportunity to validate the method of CSM generation by a UAV under different conditions than in Germany. The aim of this study is to monitor plant growth using point clouds generated from very high resolution stereo images captured by a UAV-system.

2 DATA AQUISITION

2.1 STUDY AREA AND DATASET

The study area is Keyansuo experiment field in China's Sanjiang Plain the northern most rice growing region in China (Figure 1). Two cultivars of rice seedlings were transplanted in May of 2012. Ground water was used for constant irrigation during the growing season. Harvest of the crops took place at the end of September. The experiment consisted of 54 small plots with a size of 7 x 8 m, in which three replications of the rice varieties Kongyu131 and Longjing21 were planted in randomized order. Different amounts of N-fertilizer (0-160 kg ha^{-1}) were applied (Figure 2). The total size of the field is 0.39 ha.

In July 2012 three UAV-campaigns (04./09./17.07.12) were carried out. 30 Ground Control Points (GCP) were distributed evenly across the field to facilitate ground truth. Additional destructive sampling of biomass and non-destructive measurements of plant height, hyperspectral point data using an ASD FieldSpec and 3D point clouds using a terrestrial laser scanner were carried out.

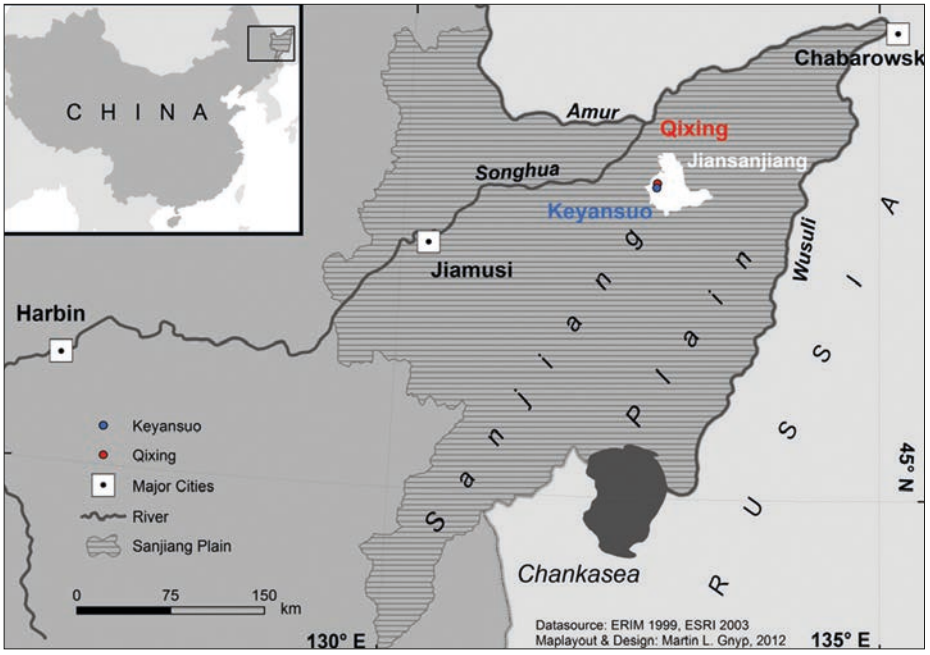

Figure 1: Location of the experiment fields Qixing and Keyansuo, Jiansanjiang Branch Bureau, Heilongjiang Bureau of Agricultural Reclamation, Heilongjiang province, China (Yu et al. 2013)

2.2 PLATFORM

The sensor platform is the MK-Okto by Hisystems (Hisystems GmbH 2013). The UAV-system was self-built at the study site in 2011. Thus on-site maintenance was pos-

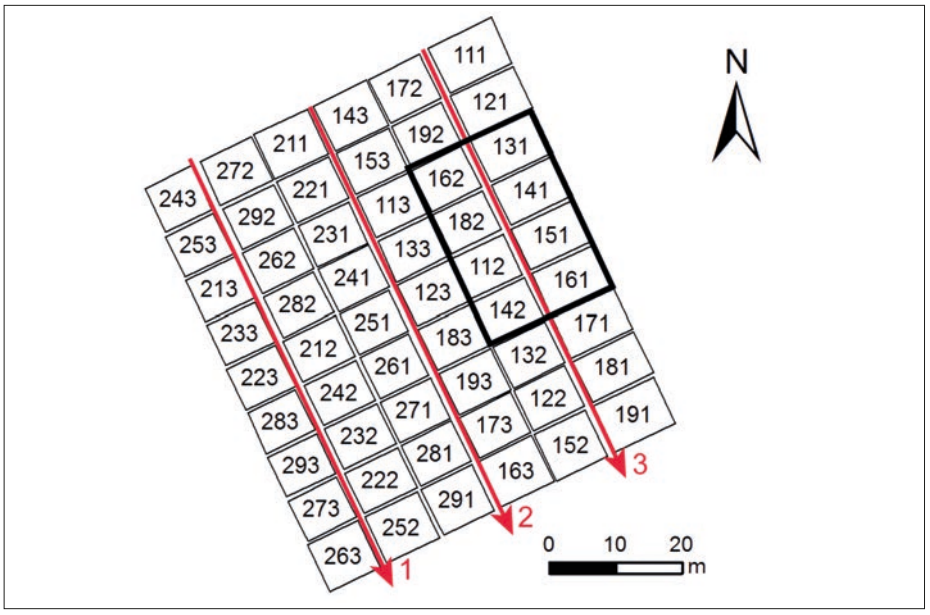

Figure 2: Experiment field in Keyansuo. Plot numbering: 1st no.: Cultivar (1 = Kongyu131, 2 = Longjing21), 2nd no.: Treatment (1 = 0, 2 = 70, 3 = 100, 4 = 130, 5 = 160 kg ha^{-1}, 6-9 = other), 3rd no.: Replication, red arrows: flight strips 1-3, black rectangle: dataset selection b.

Figure 3: MK-Okto by Hisystems GmbH mounted with Lumix DMC GF3 optical camera (Bendig et al. 2013)

sible, which is important in remote areas where spare parts and manufacturer's support might not be available. The frame consists of aluminum and fiberglass reinforced plastics (Figure 3). The eight brushless outrunner high torque engines are equipped with high performance propellers. The electronics consist of an ARM-processor equipped mainboard and a navigation mainboard with gyroscopes, a pressure sensor and a compass module (Bendig et al. 2012). Lithium polymer batteries (up to 5.000 mAh capacity) are used for the power supply. A 2.4 GHz transmitter remote control (RC) is used for stirring and camera triggering. The maximum payload is 1 kg. The average endurance is 15 minutes (about 0.5 kg payload). The price of the system including spare batteries and RC is approximately 3.000 €. The operation is possible up to a wind speed of 19 km h^{-1} (Beaufort scale number 3 for wind speed).

2.3 SENSOR

The RGB sensor used in this study is the Panasonic Lumix DMC GF3 in combination with a Lumix G 20 mm (F1.7 ASPH) fixed lens. The weight is 400 g, the sensor resolution is 4.016 x 3.016 (12 million) pixel (Panasonic 2013). Thus capturing very high resolution images of e. g. 0.01 m at a 50 m object distance is feasible. The Field of View (FOV) has an extend of 48.5° horizontal and 33.4° vertical, resulting in an image size of 45 x 30 m at a 50 m object distance.

Prior to each flight aperture and exposure time are adjusted and fixed manually according to the current light conditions. The camera gimbal is custom-built and features a mechanical trigger driven by a servomotor. The image acquisition is controlled by the remote control of the UAV-system.

2.4 MEASUREMENT

A number of 30 GCP were installed on the experiment in a uniform distribution. In order to be able to use the same GCP during the whole campaign, wooden poles were installed on the dikes. 0.3 x 0.3 m highly visible targets were attached to the poles and served as the GCP. The GCP positions were measured with a TrimbleProXT GPS with a 1 m accuracy in x-y-z-direction. For technical reasons, no more accurate device was available.

The flights were carried out at a height of 50 m, resulting in three flight strips with a 44% side and 90% forward overlap in order to cover the whole experiment field

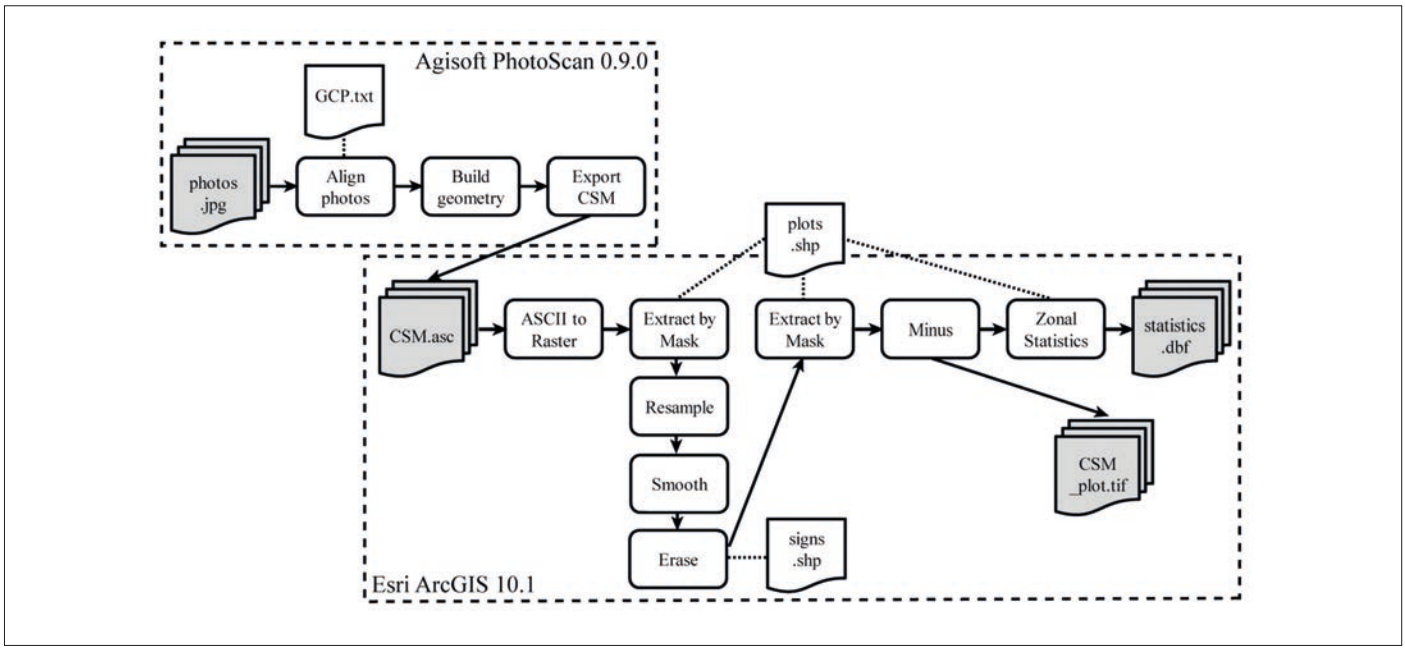

Figure 4: Data processing workflow for generation of CSM (CSM.asc) from RGB images captured by UAV-system (photos.jpg) in Agisoft PhotoScan 0.9.0 and further processing for analysis in Esri ArcGIS 10.1

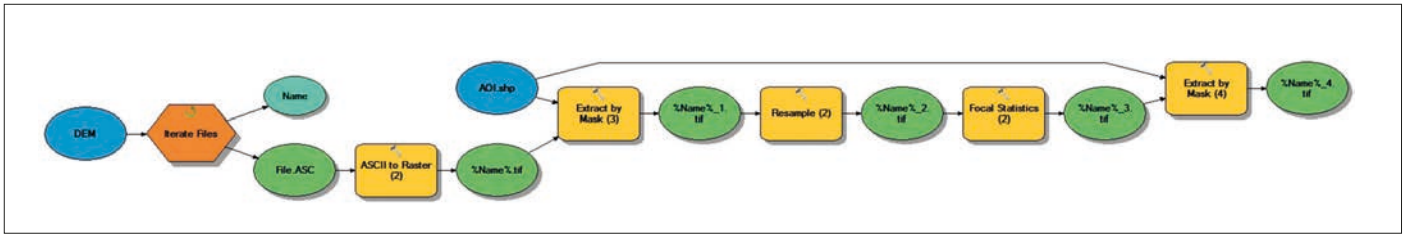

Figure 5: Model 1 in Esri ArcGIS 10.1 processing workflow – data conversion, masking and resampling

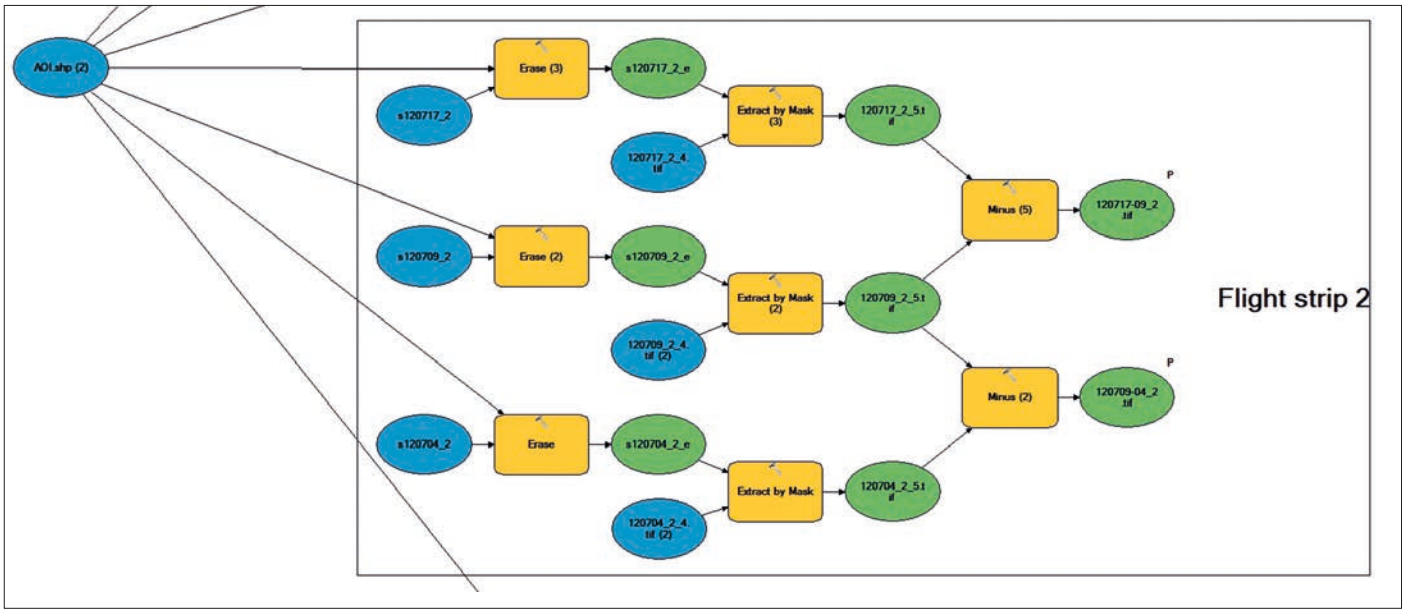

Figure 6: Model 2 in Esri ArcGIS 10.1 processing workflow – AOI refinement by applying individual masks and dataset subtraction

(Figure 2). Each flight strip was captured in a separate flight due to the endurance of the UAV-system limited by the battery capacity. The RGB sensor was mounted in a fixed nadir position and orientation.

The flights were carried out in mostly clear sky conditions (0-2 Okta) at low wind speed (up to 3.4 m/s) in the early morning between 05:30 and 07:00 am. Due to the uniform time zone in China, the sun rises at about 03:00 am in Jiansanjiang, resulting in high air temperatures in the summer between 25 °C and 35 °C in the early morning.

3 DATA PROCESSING

The data processing workflow is divided into CSM generation using Agisoft PhotoScan 0.9.0 and post processing and analysis in ArcGIS 10.1. The workflow is presented in Figure 4. The individual steps of the data analysis are described below.

3.1 AGISOFT PHOTOSCAN

The images captured during the flight campaigns were processed into CSM using the multi-view 3D reconstruction software Agisoft PhotoScan 0.9.0 (latest version 0.9.1, Agisoft LLC 2013). The software utilizes a Structure from Motion (SfM) algorithm (Verhoeven et al. 2012). This approach allows for computation of the relative projection geometry and 3D points by using only corresponding image features occurring in a series of overlapping images of the area of interest (Szeliski 2011). The surface geometry is reconstructed by using multi-view stereo (MVS) algorithms (Scharstein & Szeliski 2002, Seitz et al. 2006). The software computes a depth estimate, in this case the distance from the camera to the object surface, for nearly every pixel of each view. One view equals one image. The resulting independent depth maps are combined and approximated by a triangular mesh, resulting in a DSM (Verhoeven et al. 2012). The transformation from local to an absolute UTM coordinates was carried out by assigning the coordinates of the GCP to the corresponding images. Computation of the CSM was carried out using the highest possible accuracy resulting in computation times of up to two hours on an 8 GB RAM 64-bit operating system. The dataset for every date was divided into three tiles according to the three flight strips. This allowed for manageable size of datasets. The CSM with a 0.01 m resolution have 700 points per m^2 on average. Agisoft offers various ways of exporting the generated CSM. In this case an ASCII-file was chosen which enabled further processing in ArcGIS.

3.2 ARCGIS

Esri's ModelBuilder was used for data processing in ArcGIS 10.1. The processing steps were split up into three models due to identification signs that had been placed in the plots. Those had to be removed in each dataset by applying a mask.

Model 1 comprises data conversion, masking and resampling (Figure 5). The *File Iterator* was used to process all files (three files for each of the three dates) automatically. The *ASCII to Raster* tool was used for data conversion to a floating-point raster for enhanced performance in ArcGIS.

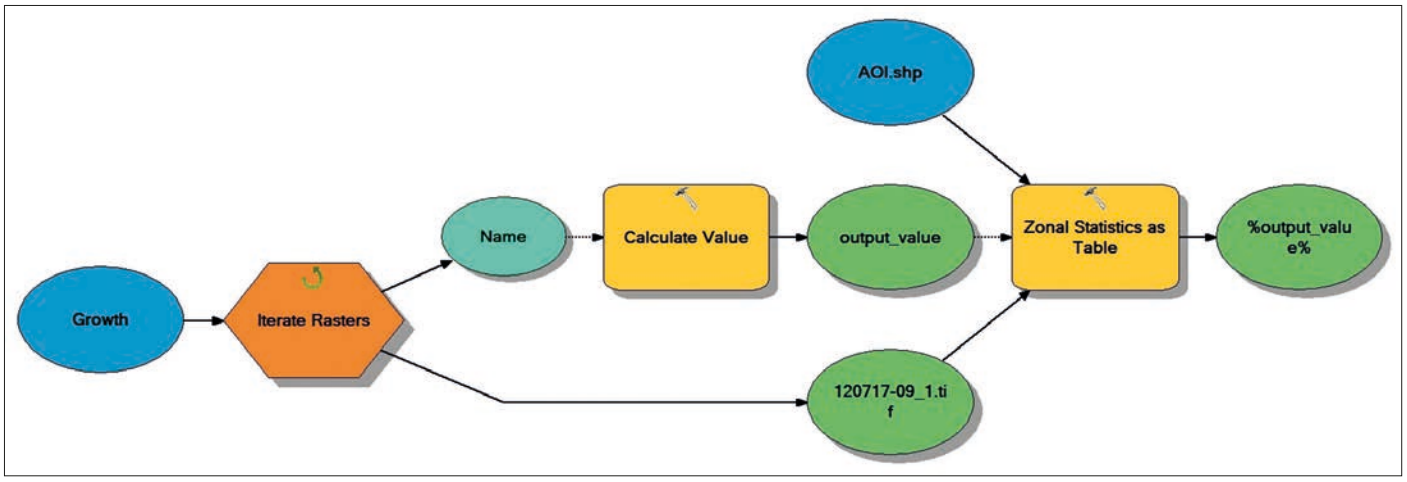

Figure 7: Model 2 in Esri ArcGIS 10.1 processing workflow – calculation of plant growth on a plot sized basis

Based on the plot boundaries visible in the CSM, a shapefile of the Area of Interest (AOI) was constructed. Plant growth at the margins of a field differs from plant growth in the middle of the field due to different environmental conditions such as availability of light. Thus a negative buffer of 0.6 m was applied to the plot boundary shapefile in order to exclude those plants from the analysis. The resulting mask was used as an input for the *Extract by Mask* tool. Results of this step were marked with a "_1" in the filename (Figure 5). In a next step the *Resample* function with a nearest neighbour interpolation was applied reduce to the cell size of the CSM to 0.1 m as it is suitable for analysis on a plant level. Outliers in the data were removed by applying the *Focal Statistics* tool with a focal mean of 3 x 3 pixel rectangles. Finally the AOI mask needed to be applied again, as the interpolation and smoothing added some pixel at the boundaries of the dataset.

In order to remove the identification signs in the field individual shapefiles containing the outlines of the signs were produced for every CSM (see e. g. s120717_2 in Figure 6). The shape of the files varied in every flight strip, due to the different viewing angles. Using the *Erase* tool the AOI mask could be modified for every single CSM (e. g. s120717_2e in Figure 6). In a next step the *Extract by Mask* tool was applied and datasets of the different dates could be subtracted from each other using the *Minus* tool. As a result the relative plant growth in meters between the 09th and 04th of July and the 17th and 09th of July can be obtained. The concept of CSM includes generation of absolute plant heights as well as growth monitoring. Due to frequently varying water levels in each of the 54 plots, no ground plane could be generated. In a barley field for example this ground plane can used as a basis for calculation of absolute heights (Bendig et al. 2013).

In a last step, plant growth on a plot sized basis was calculated using the *Zonal Statistics as Table* tool (Figure 7). The *Raster Iterator* helped to automate the process. As a result, a *.dbf-table for each dataset containing range of values, minimum, maximum, mean value and standard deviation

Dataset	All values		Selection a		Selection b	
Growth	GP1	GP2	GP1	GP2	GP1	GP2
Min	–0.433	–0.514	–0.322	–0.284	–0.019	0.078
Max	0.508	0.786	0.408	0.474	0.324	0.474
Range	0.941	1.300	0.730	0.758	0.343	0.396
Mean	0.144	0.069	0.130	0.143	0.206	0.255
Std.	0.040	0.051	0.037	0.040	0.026	0.036

Table 1: Descriptive statistics of plant growth [m] derived from CSM for all data and selected datasets a and b for two growth periods in July 2012

Cultivar		Kongyu131	Longjing21	Kongyu131	Longjing21
Growth		GP1		GP2	
Dataset	All values	0.129	0.157	0.083	0.121
	Selection a	0.129	0.131	0.155	0.129
	Selection b	0.206	no data	0.255	no data

Table 2: Mean plant growth [m] of rice cultivars Kongy131 and Longjing21 derived from CSM for all data and selected datasets a and b for two growth periods in July 2012

was generated. The tables were named according to the corresponding raster file using the *Calculate Value* function. Further analysis of the tables was carried out in Microsoft Excel.

4 RESULTS

The results of the CSM generation and the analysis of the plant growth are presented below. Analysis was carried out for three dataset selections (*all values*, *selection a* and *selection b* in Table 1, Table 2) and two growth periods (GP1 = 04.-09.07.; GP2 = 09.-17.07.). A visible inspection of the CSM showed that unrealistic height values existed in parts of single CSM (GP1: flight strip 1; GP2: flight strip 2) due to the quality of the georeference. The values of the affected plots were removed from the analysis resulting in dataset *selection a* (Table 1, Table 2). Furthermore, data at the beginning and the End of the flight strips were removed with only the core part of the field remaining. This resulted in *selection b* (see Figure 2) containing only the values where the CSM for GP1 and GP2 showed the most reliable results and were less prone to boundary effects (Figure 10).

4.1 STATISTICS

The range of overall plant growth (Table 1) obtained from the CSM is 1.3 m for the dataset containing *all values* showing negative values of up to –0.5 m. For the *selections a* and *b* show lower values of 0.7 m and 0.5 m apply. Negative values also occur (a: –0.322, b: –0.019). Regarding the mean plant growth, the datasets show differing tendencies. In the dataset with *all values*, the mean plant growth declines between GP1 and GP2 from 0.144 to 0.069 m, while for *selections a* and *b* the growth increases slightly (a: 0.13 to 0.143 m, b: 0.206 to 0.255 m). The standard deviation varies between 0.02 and 0.05 m with a mean of 0.04 m.

Table 2 shows the mean plant growth differentiated by the two cultivars of the experiment field; Kongyu131 and Longying21. In the dataset containing *all values* the growth of Longjing21 (0.157 and 0.121 m) is 31% higher than for Kongyu131 (0.129 and 0.083 m) for both GPs. In dataset *selection a*, growth only differs by less than a centimetre for GP1 but is 0.014 m higher for Kongyu131 in GP2. *Selection b* only contains data for Kongyu131 but has a 78% higher growth of 0.2 m and higher compared to the rest of the values.

4.2 CROP SURFACE MODELS

The CSM of flight strip to of the 09th of July with a 0.01 m resolution is shown in Figure 8. 27 of the 54 experiment plots are completely covered in the model. Orange areas indicate high and green areas indicate low heights. The highest areas are located in the centre of the field, while heights decrease towards the north, south and to the west. The pointy objects in red show the positions of the identification signs that had been placed in the field. The water channels used for irrigation at the northern and southern ends of the field are clearly marked by the dark green colour indicating the lowest parts of the CSM.

4.3 CROP GROWTH

A map of the plant growth of GP1 for flight strip 2 is presented in Figure 9. Values under –0.08 m are coloured in grey indicating a "negative growth" (see section 5 for discussion). Positive values change from yellow to red, with red indicating the highest growth. Areas with the highest growth between 0.2 and 0.4 m are located in the centre. Growth is decreasing towards north and south where the grey areas are located. The trend is similar to the one in Figure 8.

An example of a detailed plot analysis of dataset *selection b* is given in Figure 10 showing the plots in centre of flight strip 3. The plant growth for GP1 is shown on the left and for GP2 on the right. In general, growth for GP1 is lower than for GP2 (compare Table 2). For GP1 plots 182, 141 and 142 have the highest growth, while plot 171 has the lowest values. GP2 gives a different impression with plots 131, 182, 141 and 151 showing the highest values and 161 having lowest values. Growth variability in the plots for both GPs can be detected; for example the north western corners of plots 141 and 171 growing stronger than the south eastern corners.

5 DISCUSSION

The GCP used during the data acquisition helped during data processing with sufficient visibility and distribution across the experiment field. A strong disadvantage was that for measurement of the GCP positions, only a GPS with a low accuracy of 1 m on all three axes was available. This can be regarded as the main source of error during the process of CSM generation and the results of the whole data analysis.

The flight plan with 44% side and 90% forward overlap and 50 m flying height produced images at very high resolution with sufficient overlap for CSM generation. Comparable studies use similar flight plans with overlaps of 70% to 95% (Haala &

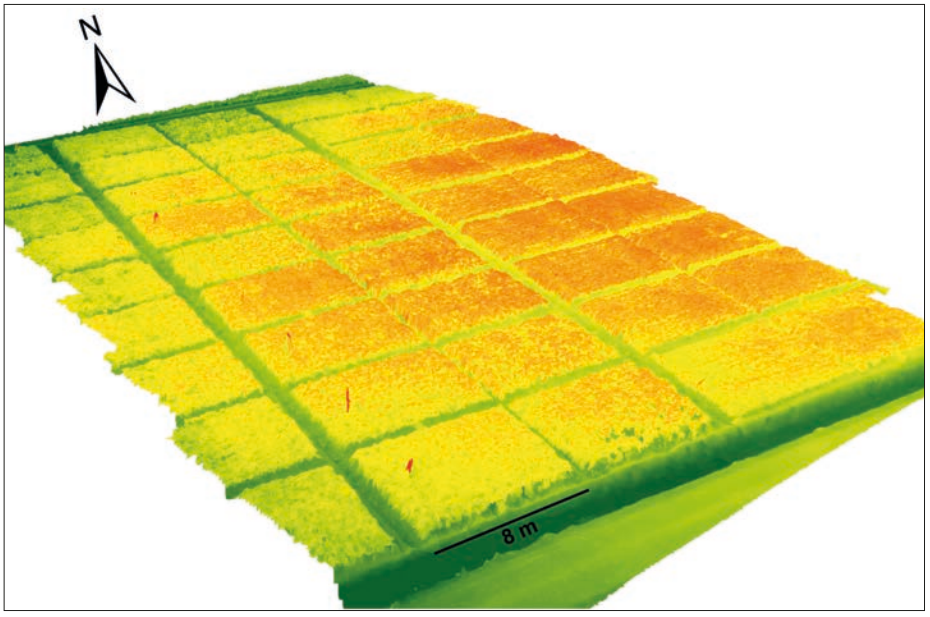

Figure 8: CSM of flight strip 2 of the 09th of July 2012 – orange areas indicate high and green areas indicate low heights (Esri ArcScene, height 2 times exaggerated)

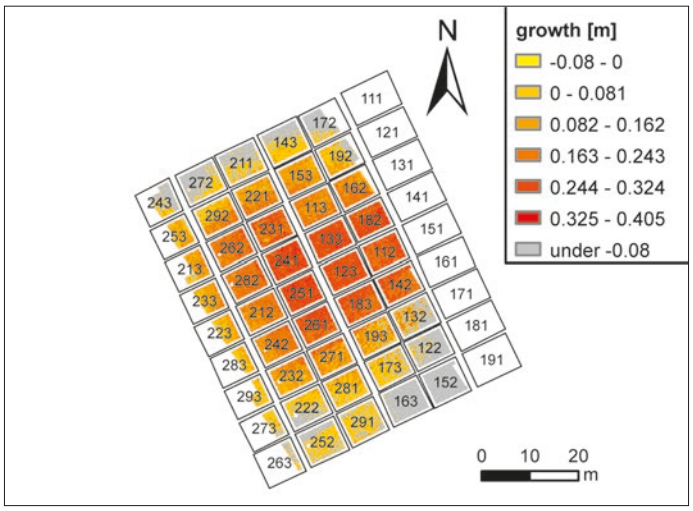

Figure 9: Plant growth in flight strip 2 between the 04th and 09th of July 2012 (GP1) (Esri ArcMap)

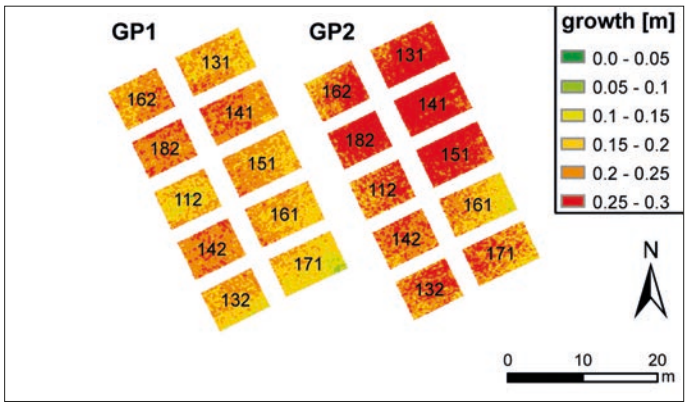

Figure 10: Plant growth of dataset selection b between the 04th and 09th of July (GP1) and the 09th and 17th of July (GP2) 2012 (Esri ArcMap)

Rothermel 2012, Hartmann et al. 2012). The area of image acquisition should be extended further across the borders of the field to account for errors at the CSM edges.

Model generation using Agisoft PhotoScan was comfortable and well suited for the task of handling unregistered aerial images. Comparisons by Neitzel & Klonowski (2011) or Gini et al. (2013) of similar software using SfM and MVS techniques like Bundler, Patch-based Multi-view Stereo Software Version 2 (PMVS2) and the photogrammetry software Leica Photogrammetry Suite (LPS) stated the good performance of Agisoft PhotoScan.

The further processing in ArcGIS with ModelBuilder offers the advantage of an adaptable and automated processing chain. The models are clearly structured which make the process easy to understand for people unfamiliar with the workflow. The fact that only one iterator can be used in the model limits the flexibility to a certain extend. Putting the whole process into a Phyton script would have been an alternative but would not offer such a good overview of the process. A solution could be building a custom made ArcGIS tool for the whole process. But more experience on processing chains for different datasets is needed first before automating processing to such an extent.

Results of the plant growth analysis show that there is a big range of values of up to one meter (see Table 1) in the dataset, which is linked to the quality of the resulting CSM; since range of values in datasets of *selection a* and *b* are considerably lower (Table 1). The fact that negative values of up to –0.5 m occur in the data evinces the limited quality of the CSM. Again, the occurrence of such values is directly linked to the low accuracy of the GCP measurement.

Values obtained for the mean plant growth still have a realistic magnitude between 0.06 and 0.26 m (Table 1) for the regarded phenological stage. This can be stated due to frequent observation of rice fields in this region since 2007 (Yu 2013).

When comparing the two rice cultivars Kongyu131 and Longjing21, no significant differentiation in growth can be observed (Table 2). Differences are in the magnitude of a few centimetres (e. g. 0.129 m compared to 0.157 m). The dataset where *all values* had been used suggests a higher growth for Longjing21, while in *selection a* the growth is higher for Kongyu131 in GP2. In-field measurements showed that Kongyu131 tends to grow slower than Longjing21. This could not be proved from the data in this paper. Either no actual difference in the growth of the two cultivars existed for the regarded GPs (about 1 month) or the quality of the CSM was not sufficient to show such differences.

When analysing the spatial distribution of growth (Figure 8, Figure 9) it can be clearly seen that plant heights are decreasing towards the northern and southern ends of the fields. This could be due to inhomogeneity in the field e. g. soil quality or other factors influencing plant growth. Since Figure 9 gives the impression of a radial decrease of growth towards the edges, another reason is more likely: It could be a barrel effect in the CSM which is resulting in lower heights at the edges of the CSM. This problem can be addressed by extending the area of interest during the flights and by solving the problem of inaccurate registration of the GCP.

In the centre of the field where this effect is less masking the true infield variability, the variability of growth in the plots can be shown with very high detail (Figure 10). This proves that the method is suitable for detection of small scale variability (here: 0.1 m raster resolution) in plant growth.

6 CONCLUSION

Choosing a UAV for monitoring a remote small sized study area like the one presented here, enables multi-temporal data acquisition at very low cost and with high flexibility. This flexibility is especially important for areas which are difficult to access such as irrigated rice fields.

Due to the strong barrel effect influencing the models, no analysis of the different treatments of N-fertilizer (Figure 2) was performed. This step can be added to the analysis as well as comparison of the derived CSM with the additional data available such as CSM from terrestrial laser scanning, hyperspectral reflection data and agronomical data collected for the same time span.

In summary it can be stated that the method of multi-temporal CSM generation from UAV-based data, is applicable to rice. For the reliable modelling of plant growth and a differentiation of cultivars

and treatment the model quality needs to be improved, which is possible through improved post processing.

7 OUTLOOK

Although the platform is performing well, some improvements are possible. A gimbal enabling pitch and roll compensation during the flight was mounted. A camera with a higher image resolution (Panasonic Lumix DMC GX1, 16 M pixel) is used. It is triggered electrically, which has the advantage of a more reliable image acquisition. Another advantage is continuous image acquisition which guarantees an over 95% forward overlap.

The availability of point clouds generated from terrestrial laser scanning offers the chance of using the highly precise local coordinate system for georeferencing of the CSM resulting in models of significantly higher accuracy. This will greatly improve the usability of the resulting CSM and offer wider possibilities of data analysis.

References

Agisoft LLC (2013): Image-based 3D modeling. Make it with Agisoft PhotoScan. http://www.agisoft.ru, accessed 9/2013.

Bendig, J.; Bolten, A.; Bareth, G. (2012): Introducing a low-cost Mini-UAV for thermal- and multispectral-imaging. In: International Archives of the Photogrammetry, Remote Sensing and Spatial Information Sciences, XXXIX (B1), pp. 345-349.

Bendig, J.; Bolten, A.; Bareth, G. (2013): UAV-based imaging for multi-temporal, very high resolution crop surface models (CSMs) to monitor crop growth variability. In: Photogrammetrie – Fernerkundung – Geoinformation (PFG), 6/2013, pp. 551-562.

Berni, J. A. J.; Zarco-Tejada, P. J.; Suárez, L.; Fereres, E. (2009): Thermal and narrowband multispectral remote sensing for vegetation monitoring from an unmanned aerial vehicle. In: IEEE Transactions on Geoscience and Remote Sensing, 47 (3), pp. 722-738.

Gini, R.; Pagliari, D.; Passoni, D.; Pinto, L.; Sona, G.; Dosso, P. (2013): UAV photogrammetry: block triangulation comparisons. In: International Archives of the Photogrammetry, Remote Sensing and Spatial Information Sciences, XL-1/W2, pp. 157-162.

Haala, N.; Rothermel, M. (2012): Dense multi-stereo matching for high quality digital elevation models. In: Photogrammetrie – Fernerkundung – Geoinformation, 4/2012, pp. 331-343.

Hansen, P. M.; Schjoerring, J. K. (2003): Reflectance measurement of canopy biomass and nitrogen status in wheat crops using normalized difference vegetation indices and partial least squares regression. In: Remote Sensing of Environment, 86 (4), pp. 542-553.

Hardin, P. J.; Jensen, R. R. (2011): Introduction – Small-scale unmanned aerial systems for environmental remote sensing. In: GIScience & Remote Sensing, 48 (1), pp. 1-3.

Hartmann, W.; Tilch, S.; Eisenbeiss, H.; Schindler, K. (2012): Determination of the UAV position by automatic processing of thermal images. In: International Archives of the Photogrammetry, Remote Sensing and Spatial Information Sciences, XXXIX (B6), pp. 111-116.

Hendrickx, M.; Gheyle, W.; Bonne, J.; Bourgeois, J.; De Wulf, A.; Goossens, R. (2011): The use of stereoscopic images taken from a microdrone for the documentation of heritage – An example from the Tuekta burial mounds in the Russian Altay. In: Journal of Archaeological Science, 38, pp. 2968-2978.

Hisystems GmbH (2013): http://www.hisystems.de, accessed 09/2013.

Hoffmeister, D.; Bolten, A.; Curdt, C.; Waldhoff, G.; Bareth, G. (2010): High resolution Crop Surface Models (CSM) and Crop Volume Models (CVM) on field level by terrestrial laserscanning. In: SPIE Proceedings, 7840.

Miao, Y.; Stewart, B. A.; Zhang, F. (2012): Long-term experiments for sustainable nutrient management in China. A review. In: Agronomy for Sustainable Development, 31, pp. 397-414.

Martinsanz, G. P. (2012): Special issue "Unmanned Aerial Vehicles (UAVs) based remote sensing". https://www.mdpi.com/journal/remotesensing/special_issues/uav, accessed 09/2013.

Mulla, D. J. (2012): Twenty five years of remote sensing in precision agriculture: Key advances and remaining knowledge gaps. In: Biosystems Engineering, XXX, pp. 1-14.

Neitzel, F.; Klonowski, J. (2011): Mobile 3D mapping with a low-cost UAV system. In: International Archives of the Photogrammetry, Remote Sensing and Spatial Information Sciences, XXXVIII-1 (C22), pp. 1-6.

Panasonic (2013): http://94.23.55.209/index.php/Cameras/Camera-Sensor-Database/Panasonic/Lumix-DMC-GF3, accessed 09/2013.

Scharstein, D.; Szeliski, R. (2002): A taxonomy and evaluation of dense two-frame stereo correspondence algorithms. In: International Journal of Computer Vision, 47, pp. 7-42.

Seitz, S. M.; Curless, B.; Diebel, J.; Scharstein, D.; Szeliski, R. (2006): A comparison and evaluation of multi-view stereo reconstruction algorithms. In: 2006 IEEE Computer Society Conference on Computer Vision and Pattern Recognition (CVPR'06), 1/2006, 519-528.

Szeliski, R. (2011): Computer Vision. Algorithms and Applications. Springer-Verlag, Berlin/Heidelberg/New York, pp. 307-314.

Thenkabail, P. S.; Smith, R. B.; Pauw, E. D. (2000): Hyperspectral vegetation indices and their relationship with agricultural crop characteristics. In: Remote Sensing of Environment, 71 (2), pp. 152-182.

Verhoeven, G.; Doneus, M.; Briese, C.; Vermeulen, F. (2012): Mapping by matching: a computer vision-based approach to fast and accurate georeferencing of archaeological aerial photographs. In: Journal of Archaeological Science, 39, pp. 2060-2070.

Yu, K.; Li, F.; Gnyp, M. L.; Miao, Y.; Bareth, G.; Chen, X. (2013): Remotely detecting canopy nitrogen concentration and uptake of paddy rice in the Northeast China Plain. In: ISPRS Journal of Photogrammetry and Remote Sensing, 78, pp. 102-115.